Copyright (2012) American Institute of Physics. This article may be downloaded for personal use only. Any other use requires prior permission of the author and the American Institute of Physics.

*The following article appeared in (**J. Chem. Phys.**, **137**, 214505, **2012**) and may be found at (http://link.aip.org/link/?JCP/137/214505).*

Liquid-liquid transition in ST2 water

Yang Liu, Jeremy C. Palmer, Athanassios Z. Panagiotopoulos, and Pablo G. Debenedetti[a)]
Department of Chemical and Biological Engineering, Princeton University, Princeton, New Jersey 08544, USA

(Received 9 October 2012; accepted 13 November 2012; published online 6 December 2012)

We use the weighted histogram analysis method [S. Kumar, D. Bouzida, R. H. Swendsen, P. A. Kollman, and J. M. Rosenberg, J. Comput. Chem. **13**, 1011 (1992)] to calculate the free energy surface of the ST2 model of water as a function of density and bond-orientational order. We perform our calculations at deeply supercooled conditions ($T = 228.6$ K, $P = 2.2$ kbar; $T = 235$ K, $P = 2.2$ kbar) and focus our attention on the region of bond-orientational order that is relevant to disordered phases. We find a first-order transition between a low-density liquid (LDL, $\rho \approx 0.9$ g/cc) and a high-density liquid (HDL, $\rho \approx 1.15$ g/cc), confirming our earlier sampling of the free energy surface of this model as a function of density [Y. Liu, A. Z. Panagiotopoulos, and P. G. Debenedetti, J. Chem. Phys. **131**, 104508 (2009)]. We demonstrate the disappearance of the LDL basin at high pressure and of the HDL basin at low pressure, in agreement with independent simulations of the system's equation of state. Consistency between directly computed and reweighted free energies, as well as between free energy surfaces computed using different thermodynamic starting conditions, confirms proper equilibrium sampling. Diffusion and structural relaxation calculations demonstrate that equilibration of the LDL phase, which exhibits slow dynamics, is attained in the course of the simulations. Repeated flipping between the LDL and HDL phases in the course of long molecular dynamics runs provides further evidence of a phase transition. We use the Ewald summation with vacuum boundary conditions to calculate long-ranged Coulombic interactions and show that conducting boundary conditions lead to unphysical behavior at low temperatures. © *2012 American Institute of Physics*. [http://dx.doi.org/10.1063/1.4769126]

I. INTRODUCTION

The distinctive physical properties of liquid water[1,2] include an unusually large isobaric heat capacity compared to that of common liquids, expansion upon freezing, and negative thermal expansion below 4 °C. These characteristics exert a profound influence on the earth's physical landscape and on its climate. Furthermore, because the chemical and physical processes essential to life, as we know it, occur in an aqueous medium, the rates, mechanisms, and equilibrium states of such processes are profoundly influenced by water's physical properties.[1]

Liquid water's anomalies are exacerbated in the supercooled state, when it is metastable with respect to crystallization.[3–6] For example, the isothermal compressibility,[7–9] isobaric heat capacity,[10–14] and the magnitude of the negative thermal expansion coefficient[15–17] of supercooled water at ambient pressure increase sharply with decreasing temperature. The largest inventory of supercooled water occurs in clouds[4] and its physical properties determine the mechanisms and rates of important atmospheric phenomena such as ice formation, rainfall, and electrification.[18–21] Ever since the pioneering work of Speedy and Angell focused the attention of the scientific community on the properties of supercooled water,[7] there has been a sustained effort involving experiments, theory, and computer simulations aimed at understanding the microscopic origin and thermodynamic implications of the anomalous increase in water's response functions upon supercooling.

One interpretation of the experimental facts was proposed by Poole *et al.* 20 years ago,[22] based on computer simulations of the ST2 model of water.[23] These authors proposed that there exists in supercooled water a metastable, first-order phase transition between high-density and low-density liquid phases (HDL and LDL, respectively), which terminates at a critical point. The presence of such a critical point would explain the increase in response functions upon supercooling. According to the liquid-liquid phase transition scenario (LLPT), the experimentally-observed sharp density changes that occur between the low- and high-density forms of glassy water[24–26] are but the structurally-arrested manifestation of the LLPT. Alternative interpretations of the increase in response functions upon supercooling do not, however, invoke a LLPT.[27–29]

A phase transition between two liquid phases of the same substance involves smaller density and enthalpy changes than, say, a vapor-liquid transition. Accordingly, the characteristic energy and hence the critical temperature associated with such a liquid-liquid transition would be considerably lower than the ordinary vapor-liquid critical temperature.[30] Experimental evidence either consistent with or suggestive of a liquid-liquid transition in water[31,32] and other liquids[33–39] has, accordingly, invariably involved supercooled states.

Experimental studies aimed at substantiating or disproving the LLPT in water are especially challenging on account

a)Author to whom correspondence should be addressed. Electronic mail: pdebene@princeton.edu.

 © 2012 American Institute of Physics

Downloaded 06 Dec 2012 to 128.112.34.78. Redistribution subject to AIP license or copyright; see http://jcp.aip.org/about/rights_and_permissions

of the deep penetration into the supercooled region that would be needed in order to approach the metastable critical point. One interesting approach has been to suppress ice nucleation by confining water in hydrophilic pores of nanoscopic dimensions (e.g., Refs. 40–42). Relating the observed behavior of nanoconfined water to that in the bulk remains a challenge and renders the interpretation of such experiments far from straightforward.[43]

Theoretical progress on the subject of liquid-liquid transitions in pure substances can be classified into two broad categories. One particularly fruitful body of work has focused on the development of microscopic models whose physical parameters can be tuned so as to either exhibit a LLPT or not (e.g., Refs. 44–47). The value of such work lies in the microscopic insight that it provides as to possible molecular mechanisms that can underlie liquid-liquid phase separation in a pure substance. Equally illuminating have been studies aimed at investigating the extent to which experimental data for water (e.g., volume as a function of temperature and pressure) can be correlated with theoretically-based expressions, such as those that arise from the theory of critical phenomena.[8,48–51] The goal of this body of work, in other words, is to examine whether the existing experimental evidence is consistent (or not) with the presence of a metastable critical point.

Computer simulations have played an important role in the investigation of deeply supercooled water, beginning with the above-mentioned pioneering work of Poole *et al.*[22] Although much has been learned about the microscopic structure, transport, and thermodynamic properties of supercooled water (e.g., Refs. 52–58), it is not until quite recently that state-of-the-art methods designed specifically for the computational study of phase transitions have been deployed in the investigation of the LLPT in water. Liu *et al.*[59] used histogram-reweighting grand canonical Monte Carlo simulations[60] and showed the existence of a LLPT in the ST2 model of water[23] with Ewald summation treatment of long-ranged electrostatic interactions.[61] Sciortino *et al.*[62] obtained similar conclusions using successive umbrella sampling grand canonical Monte Carlo simulations of the ST2 model with reaction field treatment of long-ranged Coulombic interactions.[61] The ST2 potential enhances tetrahedral order and consequently exhibits anomalies, such as negative thermal expansion, up to higher temperatures than real water (atmospheric pressure density maximum at ca. 330 K in ST2 vs 277 K in real water). This allows the computational investigation of water anomalies to be conducted at higher temperatures compared to other popular force fields (e.g., SPC/E[63]), thereby avoiding prohibitively slow structural equilibration rates.[59]

Both the studies of Liu *et al.*[59] and of Sciortino *et al.*[62] were challenged by Limmer and Chandler.[64] These authors calculated the free energy surface of two models of water, as a function of density, and a bond-orientational order parameter that can distinguish crystalline from amorphous phases.[65] Limmer and Chandler used a hybrid Monte Carlo scheme in the (*N, P, T*) ensemble to propagate trajectories, umbrella sampling to control the order parameters and the multi-state Bennett acceptance ratio[66] method to unweigh the biased simulation data and estimate the free energy differences between windows. Most of the calculations performed by Limmer and Chandler pertained to the mW coarse-grained model,[67] but they also studied the ST2 model with Ewald summation treatment of long-ranged Coulombic forces. They concluded that the LLPT in ST2 water is really a liquid-crystal transition and that at no range of temperatures and pressures investigated is there more than one liquid basin. They reached similar conclusions for the mW model. The work of Limmer and Chandler is an important methodological advance. It pointed out the importance of computing the free energy not just as a function of density but also as a function of order parameters that can distinguish crystalline from amorphous states.

In addition to the above-mentioned work of Liu *et al.*[59] and of Sciortino *et al.*,[62] behavior consistent with the existence of a LLPT in ST2 water has most recently been obtained by Kesselring *et al.*,[68] who observed persistent flipping between LDL and HDL states in μs-long (*N, P, T*) molecular dynamics (MD) simulations and used finite-size scaling to locate the critical point. In light of the inconsistency between the conclusions of Limmer and Chandler[64] and those of Liu *et al.*,[59] Sciortino *et al.*,[62] and Kesselring *et al.*,[68] in this work we undertake a detailed investigation of the free energy surface of ST2 water with Ewald treatment of long-ranged Coulombic forces as a function of both density and a bond-orientational order parameter.[65] Our calculations focus on the region of bond-orientational order relevant to disordered phases and provide clear evidence of a LLPT in this model.

None of the existing classical models of water is accurate enough to answer the question of the existence or lack of a LLPT in real water. Rather, studies such as the present one provide insight into the still poorly understood but important question of what specific aspects of a force field can give rise to liquid-liquid immiscibility. It is hoped that such investigations will eventually yield a taxonomy of water force fields with respect to their ability to describe a LLPT.

We emphasize here that the conclusions arrived at in this work pertain exclusively to the ST2 model of water. In studies of the LLPT in water, our experience suggests that generalizing to other models findings that are specific to a given force field should be avoided. Thus, as will be discussed in detail in Sec. III, the LDL phase of ST2 can be fully equilibrated over times that are accessible to simulation. The interesting possibility, observed computationally in studies of the coarse-grained mW model,[69,70] and addressed also in theoretical work,[71,72] that at conditions relevant to the hypothesized LLPT the liquid phase cannot be equilibrated before crystallization occurs, needs to be ascertained for each specific model, and is of course of relevance to real water.

This paper is organized as follows: Methodological details, including definition of the model, simulation methods, and error estimates, are provided in Sec. II. Section III presents our main results and a discussion thereof. The main conclusions and suggestions for future work are presented in Sec. IV.

Downloaded 06 Dec 2012 to 128.112.34.78. Redistribution subject to AIP license or copyright; see http://jcp.aip.org/about/rights_and_permissions

II. METHODS

A. Model system

In the ST2 model,[23] each water molecule has a tetrahedral geometry, with an oxygen atom at the center and four rigidly located point charges (two fractional positive charges representing partially shielded protons and two fractional negative charges) located at the vertices. The distances to the oxygen from a partial positive charge ($q = +0.24357e$) and from a partial negative charge ($q = -0.24357e$) are 1 Å and 0.8 Å, respectively. Oxygen-oxygen interactions are described using the Lennard-Jones potential with a characteristic distance $\sigma = 3.10$ Å and a characteristic energy $\varepsilon = 0.31694$ kJ/mol. The Coulombic interactions between the charges are supplemented with a modulation function that varies smoothly between 0 at small distances ($r \leq 2.0160$ Å) and 1 at large distances ($r \geq 3.1287$ Å) and reaches 0.5 at $r = 2.5724$ Å, where r is the oxygen-oxygen distance.

In this work, as in our previous study[59] of low-temperature phase behavior in ST2 water, we supplement the original model introduced by Stillinger and Rahman[23] and described above, by accounting for long-ranged Coulombic interactions using the Ewald summation.[61] Details on the implementation of the Ewald calculations are given in Secs. II B and II C below.

B. Umbrella sampling *NPT* Monte Carlo simulations

In our study, simulations of 192 water molecules were carried out in a cubic box, under periodic boundary conditions in the x, y, and z directions. We used a cutoff at $r = 6.975$ Å ($2.25\ \sigma$) for the Lennard-Jones interactions between oxygen atoms. The standard long-range corrections for the Lennard-Jones potential using a mean field approximation were included in our calculation.[61] The long-range Coulombic interactions between the charged sites of water molecules were calculated using the Ewald summation with vacuum boundary conditions, in accordance with our previous work.[59] In the Ewald summation, the real-space sum is calculated using the minimum-image convention; the parameter describing the width of the screening charge Gaussian distribution was set to $5/L$, where L is the box length and 518 wave vectors were used in the reciprocal space sum.

Umbrella sampling calculations were performed in the *NPT* ensemble Monte Carlo simulations at two conditions: (228.6 K, 2.2 kbar) and (235 K, 2.2 kbar). The former state point is very close to coexistence conditions according to our equation of state calculations for this model (see Sec. III) and the latter state point was studied by Limmer and Chandler.[64] Following these authors, we employed the following biasing potential:

$$\Delta U = k_1(\rho - \rho^*)^2 + k_2(Q_6 - Q_6^*)^2, \tag{1}$$

where ρ is the density of the system and Q_6 is the bond-orientational order parameter,[65] which is used to distinguish crystalline from liquid configurations. ρ^* and Q_6^* are the controlled density and bond-orientational order parameter in each window. We adopted the values $k_1 = 6000\ k_BT$ (cc/g)^2, $k_2 = 2000\ k_BT$, where T is temperature and k_B is Boltzmann's constant.

The parameter Q_6 is a function of the system's averaged spherical harmonic components.[65] We first calculated the averaged spherical harmonics of each molecule i with respect to its 4 nearest neighbors

$$q_{l,m}^i = \frac{1}{4}\sum_{j\in nn_i}^{4} Y_l^m(\phi_{ij}, \theta_{ij}), \quad -l \leq m \leq l, \tag{2}$$

where $Y_l^m(\phi_{ij}, \theta_{ij})$ is the l,m spherical harmonic function of the angular coordinates of the vector joining molecules i and j. The averaged special harmonics of each molecule were then summed

$$Q_{l,m} = \sum_{i=1}^{N} q_{l,m}^i. \tag{3}$$

The bond-orientational order parameter Q_l is a rotationally-invariant quantity constructed from $Q_{l,m}$

$$Q_l = \frac{1}{N}\left(\sum_{m=-l}^{l} Q_{l,m}Q_{l,m}^*\right)^{1/2}. \tag{4}$$

The value of Q_6 is around 0.5 for crystalline configurations and changes very little with system size. For amorphous phases, Q_6 vanishes as $N^{-1/2}$, where N is the system size and takes on a small value ($\sim$0.05 in our case) in a finite system.

For the calculation of the liquid-state free energy surface, we performed simulations in 35 density windows in the range $0.9 \leq \rho^* \leq 1.24$ g/cc, in steps of 0.01 g/cc and in two Q_6 windows, with Q_6^* set to 0.05 and 0.07. In windows with 0.90 g/cc $\leq \rho^* <$ 1.0 g/cc, we performed 32 to 80 parallel independent runs per window, each with 0.2×10^9 to 10^9 steps. For windows with 1.0 g/cc $\leq \rho^* \leq$ 1.24 g/cc, we performed 20 parallel independent runs in each window and each run was about 0.2×10^9 steps. The initial configurations were prepared in two ways: (i) several long *NPT* molecular dynamics simulations were conducted at 228.6 K, 2.2 kbar and configurations spanning a broad density range were taken after the system was equilibrated for at least 60 ns. Those configurations then become the initial configurations in the corresponding MC umbrella windows, i.e., the windows with ρ^* closest to the density of the configuration, and were simulated with different seeds for generating microstates. (ii) Configurations with $\rho \sim 0.90$ g/cc from MD simulations were taken and simulated in the MC windows with $\rho^* = 0.90$ g/cc. The configurations with ρ and Q_6 in the overlapping range with the adjacent windows were then taken as initial configurations for the subsequent window. The ratio of single particle displacement, rotation, and volume change moves was N: N : 2, where N is the total number of molecules. In displacement moves, the maximum move size was $0.15\ \sigma$. In rotation moves, a randomly selected molecule was rotated by an amount uniformly distributed between $-\pi/5$ and $+\pi/5$ about one of the three space-fixed axes chosen at random. In volume moves, logarithmic volume moves were conducted and the maximum

Downloaded 06 Dec 2012 to 128.112.34.78. Redistribution subject to AIP license or copyright; see http://jcp.aip.org/about/rights_and_permissions

move size was 0.1 (in $\ln\sigma^3$). Metropolis criteria[61] were applied for accepting or rejecting moves and the acceptance ratio was about 20%–30% for all types of moves. After equilibrium was reached, histograms in the (U, ρ, Q_6) space were generated and combined using weighted histogram analysis method techniques[73] to obtain a global free energy surface in the (ρ, Q_6) space at conditions of interest.

In order to make sure that the free energy surface obtained represents true equilibrated results rather than non-equilibrium artifacts, we performed histogram self-consistency checks in two different ways: (a) histograms at (228.6 K, 2.2 kbar) were constructed first using only the data at (228.6 K, 2.2 kbar). This was compared to the histograms obtained by combining only the data at (235 K, 2.2 kbar) reweighted to (228.6 K, 2.2 kbar). The consistency of histograms at (235 K, 2.2 kbar) was also checked by comparing them with histograms obtained at (228.6 K, 2.2 kbar) and reweighted to (235 K, 2.2 kbar). As will be shown in Sec. III, the agreement between original and reweighted histograms was excellent. (b) Because the LDL phase has much slower relaxation rates than the HDL phase, it deserves careful examination; we took a few configurations generated from MC simulations in the HDL windows (1.13 g/cc $\leq \rho^* \leq$ 1.16 g/cc) as initial configurations for the umbrella sampling simulations performed in LDL windows in the range of $0.9 \leq \rho^* \leq 0.94$ g/cc with the corresponding biased potentials, ran with different seeds, and recalculated the free energy surface using only those runs starting from HDL densities. Each simulation was equilibrated for at least 500×10^6 steps before data were collected. As will be shown in Sec. III, excellent agreement between the free energy surfaces was obtained.

The uncertainties of the free energy surface were calculated by grouping the independent runs in each window randomly into four subgroups and calculating the free energy surface using only runs in the same group. The uncertainties were therefore the standard deviations of the four independent calculations. The simulations required a total of approximately 30 central processing unit years on 3 GHz Xeon processors.

C. *NVT* and *NPT* molecular dynamics simulations

We also performed *NVT* and *NPT* molecular dynamics simulations at (228.6 K, 2.2 kbar), for sample initialization, equation of state calculations, and phenomenological phase-flipping observations. In order to avoid force discontinuities due to the truncation of the intermolecular potentials, we adopted the procedure of Ref. 74 to describe intermolecular interactions. Specifically, we added a switching function to the Lennard-Jones potential

$$U_{LJ}(r) = \sum u_{LJ}(r) S(r) + U_{LJ,tail}, \tag{5}$$

where $u_{LJ}(r)$ is the Lennard-Jones function and $S(r)$ is a polynomial function of $Z(r) = r^2 - R_{lower}^2$

$$S(Z(r)) = \begin{cases} 1 & if \quad r \leq R_{lower} \\ 1 + AZ^3 + BZ^4 + CZ^5 & if \quad R_{lower} < r \leq R_{upper}, \\ 0 & if \quad r > R_{upper} \end{cases} \tag{6}$$

with $A = -10/D^3$, $B = 15/D^4$, $C = -6/D^5$, and $D = R_{upper}^2 - R_{lower}^2$. The cutoffs in the switching functions R_{lower} and R_{upper} were taken as 7.25 Å and 7.75 Å, respectively. The long range correction for the Lennard-Jones interactions $U_{LJ,tail}$ involves weighted integrals of $u_{LJ}(r)$ over the ranges $R_{lower} \leq r \leq R_{upper}$ or $r \geq R_{upper}$, which are documented in Eq. (6) in Ref. 74.

The real space of the Ewald summation was calculated using the same modulation function and cutoffs as for the LJ potentials. In the reciprocal space, 2242 wave vectors were used and the parameter describing the width of the screening charge Gaussian distribution was set to 0.35 $Å^{-1}$. As in our previous work,[59] we used vacuum boundary conditions. Temperature and pressure were controlled using the method described in Ref. 75, with the time scale parameter set to 500 fs for both the barostat and the thermostat. The molecular geometry was constrained using the RATTLE algorithm.[76]

III. RESULTS AND DISCUSSION

Figure 1 shows the (P, T) projection of the coexistence line, terminating at the previously-reported critical point,[59] and the spinodal curves. In Ref. 59 we obtained the (T, ρ) projection of the coexistence locus. The black squares in Figure 1 were obtained by performing independent MD simulations in the (N, V, T) ensemble at 223 and 228.6 K, using $N = 203$, and calculating the coexistence pressure through a Maxwell equal-area construction performed on the computed P vs V equation of state, which exhibited van der Waals loops at these two sub-critical temperatures. The coexisting densities were in excellent agreement with the previously-reported (T, ρ) projection of the binodal curve. The pressure extrema along the van der Waals loops define the spinodal curves: the LDL phase is unstable in the region above the LDL spinodal and the HDL phase is unstable in the region below the HDL spinodal. At 228.6 K, the coexistence pressure was estimated to be 2.2 kbars, which was the state point where we performed most of our simulations.

A. Free energy surface

Using (N, P, T) umbrella sampling Monte Carlo simulations, we calculated the free energy surface in the (ρ, Q_6) plane at 228.6 K and 2.2 kbar, as shown in Figure 2. The contours are 1 k_BT apart. We found two liquid basins, one centered around ρ = 1.15 g/cc and Q_6 = 0.05,

Downloaded 06 Dec 2012 to 128.112.34.78. Redistribution subject to AIP license or copyright; see http://jcp.aip.org/about/rights_and_permissions

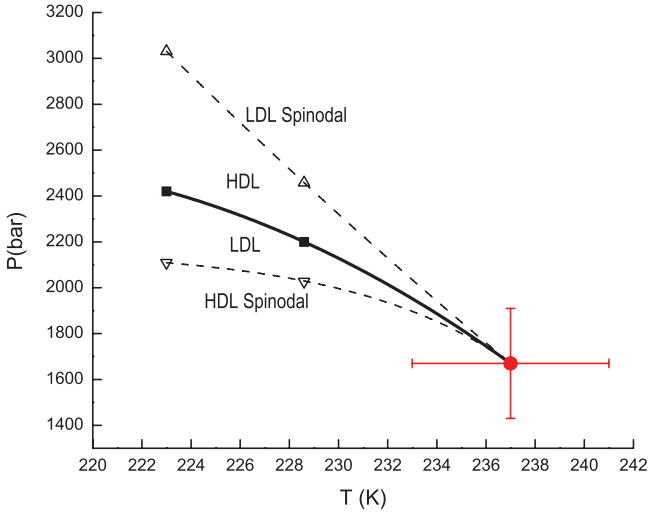

FIG. 1. (P, T) projection of the metastable phase behavior in ST2 water, showing the liquid-liquid coexistence curve (black squares), the LDL spinodal (up-triangles), and the HDL spinodal (down-triangles). Solid (phase coexistence curve) and dashed (spinodals) lines are a guide to the eye obtained by fitting the data to polynomial functions. Red circle is the critical point estimated in Ref. 59.

corresponding to the HDL phase, and the other one around $\rho = 0.91$ g/cc and $Q_6 = 0.06$, corresponding to LDL. Consistent with the highly compressible character of phases in the vicinity of a critical point, we find that the free energy surface is very sensitive to changes in pressure. Figure 3(a) shows the free energy surface at 228.6 K and 2.4 kbar. Note the disappearance of the LDL basin. Figure 3(b) shows the free energy surface at 228.6 K and 2.0 kbar. Note the disappearance of the HDL basin. These results are in a very satisfactory agreement with the independently calculated spinodal curves shown in Figure 1.

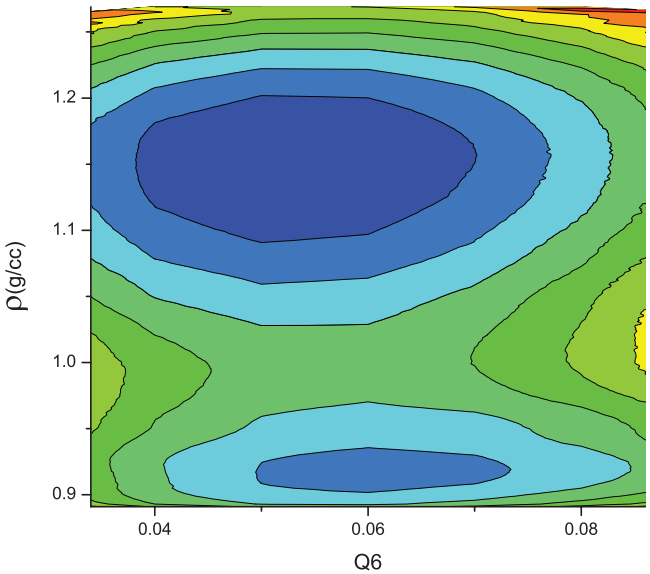

FIG. 2. Free energy surface in the (ρ, Q_6) plane at 228.6 K, 2.2 kbar. Each contour line represents 1 k_BT. Note the presence of two basins corresponding to the low- and high-density liquid phases (LDL, HDL).

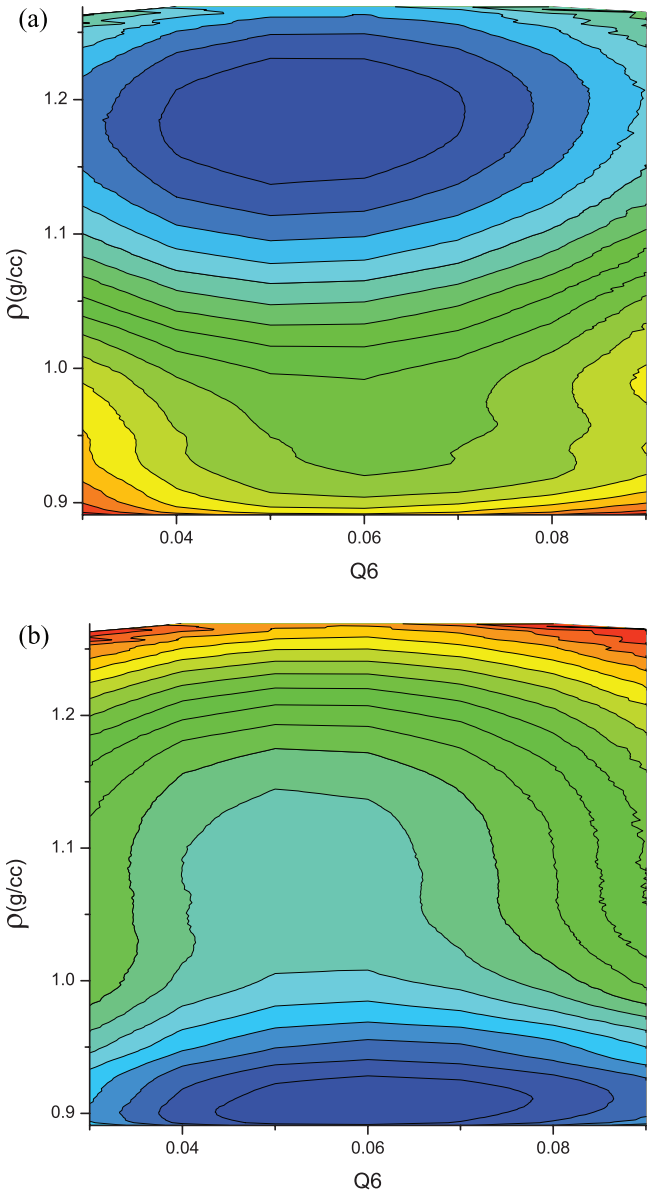

FIG. 3. Free energy surface in the (ρ, Q_6) plane at (a) 228.6 K, 2.4 kbar (b) 228.6 K, 2.0 kbar. Each contour line represents 1 k_BT. Note the disappearance of the LDL basin at high pressure (a) and of the HDL basin at low pressure (b) in agreement with the independently-calculated spinodals in Figure 1.

Figure 4 shows the density dependence of the contracted free energy at various sub-critical temperatures

$$\beta F\left(\rho, Q_6^{\max}\right) = -\ln \int_0^{Q_6^{\max}} \exp\left[-\beta F\left(\rho, Q_6\right)\right] d\, Q_6, \tag{7}$$

where $Q_6^{\max}$ is the maximum value of Q_6 considered in the calculations (0.09 for the free energy surfaces shown in Figures 2 and 3). The minima for each isotherm correspond to the equilibrium LDL and HDL phases. In agreement with the behavior reported in Ref. 59 we observe that over the range of conditions investigated here, the density of the LDL phase at coexistence changes modestly with temperature, whereas the saturated HDL phase exhibits a more pronounced density dependence. The results shown in Figures 2 and 4 are

Downloaded 06 Dec 2012 to 128.112.34.78. Redistribution subject to AIP license or copyright; see http://jcp.aip.org/about/rights_and_permissions

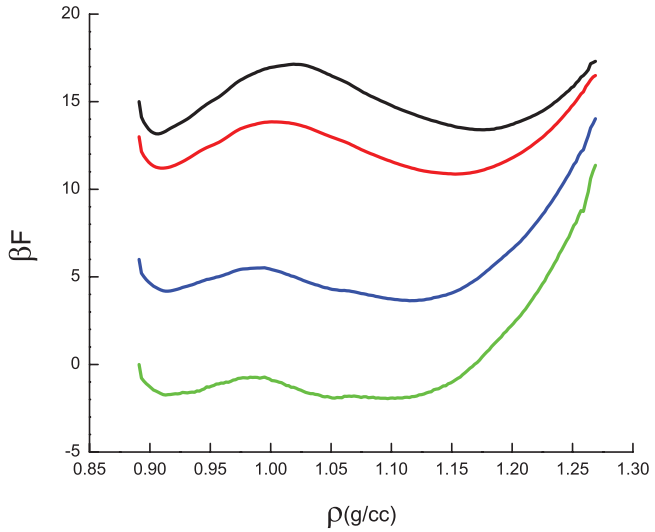

FIG. 4. Density dependence of the contracted free energy obtained by integrating over Q_6 [see Eq. (7)] at phase coexistence conditions. Black curve: 224 K, 2.3 kbar; red curve: 228.6 K, 2.19 kbar; blue curve: 235 K, 2.0 kbar; green curve: 238 K, 1.9 kbar. The relative vertical location of each isotherm is arbitrary.

consistent with free energy vs. density calculations on the ST2 model using reaction field treatment of long-ranged electrostatic interactions.[62]

Figure 5 shows the contracted free energies (βF vs ρ) at (228.6 K, 2.2 kbar: black) and at (235 K, 2.2 kbar: red). The dashed and full lines correspond to reweighted and direct calculations, respectively (dashed black = histograms obtained at 235 K and reweighted to 228.6 K; dashed red = histograms obtained at 228.6 K and reweighted to 235 K). Figure 6 shows the free energy surface at (228.6 K, 2.2 kbar), where calculations in the LDL basins were performed starting from HDL configurations generated from MC simulations that were equilibrated at high densities ($1.13 \leq \rho^* \leq 1.16$ g/cc) and biased to the LDL basin. The resulting histograms were then reweighted jointly with the same HDL-density histograms used to generate Figure 2, yielding the surface shown in Figure 6. The very good agreement between the free energy surfaces shown in Figures 2 and 6, and between the reweighted and "original" histograms shown in Figure 5, is strong proof that our calculations were fully and correctly equilibrated.

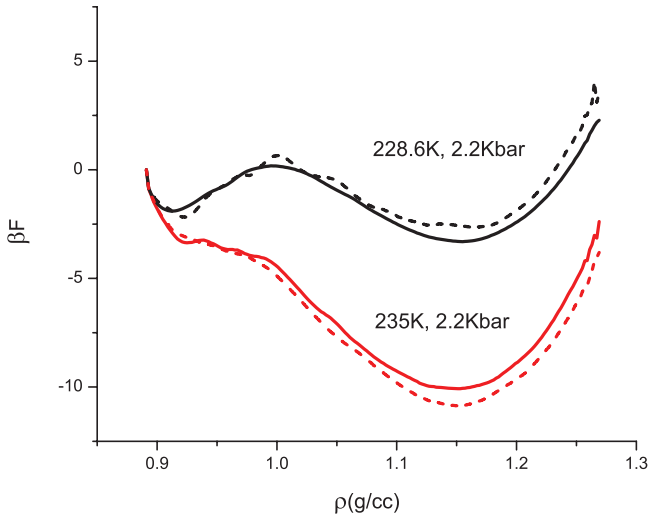

FIG. 5. Free energy as a function of density at (228.6 K, 2.2 kbar) and at (235 K, 2.2 kbar). Solid black line: 228.6 K, 2.2 kbar, using histogram data at 228.6 K, 2.2 kbar; dashed black line: 228.6 K, 2.2 kbar, using data at 235 K, 2.2 kbar (reweighted); solid red line: 235 K, 2.2 kbar, using data at 235 K, 2.2 kbar; dashed red line: 235 K, 2.2 kbar, using data at 228.6 K, 2.2 kbar (reweighted). The agreement between original and reweighted curves is an indication that the simulations properly sample equilibrated phases.

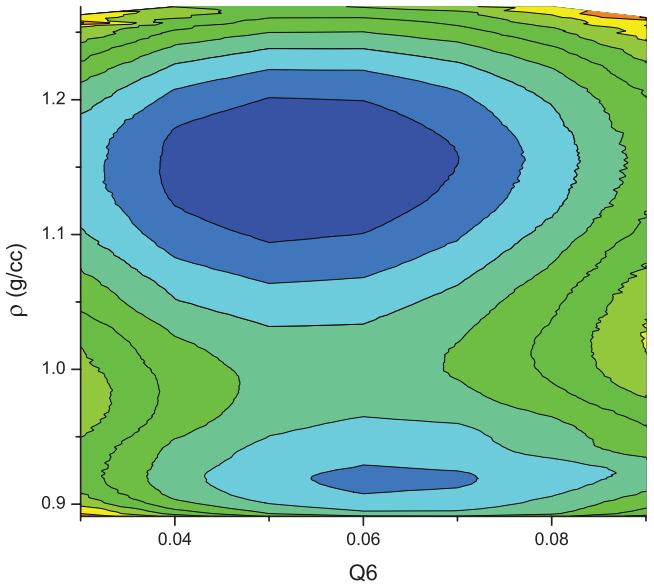

FIG. 6. Free energy surface in the (ρ, Q_6) plane at (228.6 K, 2.2 kbar), calculated with the same HDL-region histograms used to generate Figure 2 and separate LDL-region histograms obtained from simulations in the LDL windows ($0.90 \leq \rho^* \leq 0.94$ g/cc) that were first started from HDL configurations ($1.13 \leq \rho^* \leq 1.16$ g/cc) and subsequently biased to the LDL region. The agreement with the free energy surface shown in Figure 2 is an indication that the simulations properly sample equilibrated phases.

Figure 7 shows the uncertainties in the contracted free energy at 228.6 K and 2.2 kbar (see also Sec. II B).

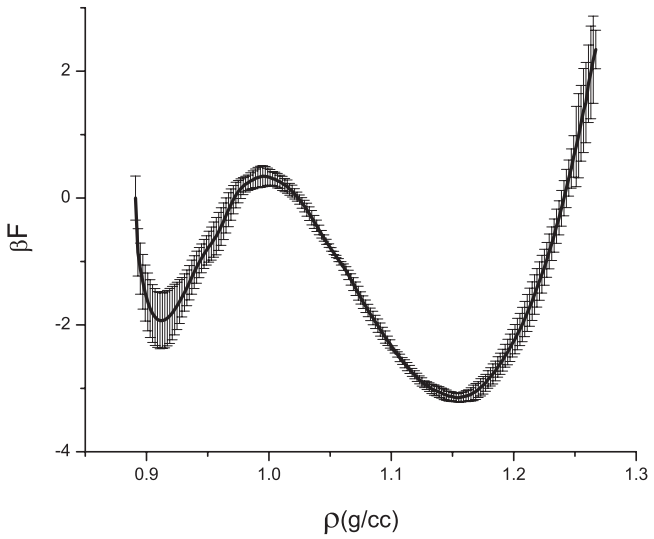

FIG. 7. Uncertainties in the calculated free energy at 228.6 K and 2.2 kbar. See text for details.

Downloaded 06 Dec 2012 to 128.112.34.78. Redistribution subject to AIP license or copyright; see http://jcp.aip.org/about/rights_and_permissions

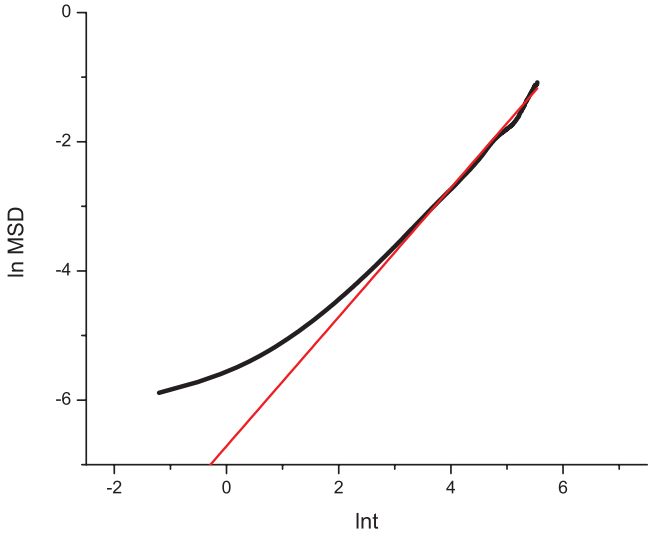

FIG. 8. "Time" dependence of the mean squared displacement of water molecules, plotted in double logarithmic coordinates, at 228.6 K, 2.2 kbar in the simulation window of $\rho^* = 0.90$ g/cc, $Q_6^* = 0.05$. Black curve is the average of 32 independent runs. The squared displacement is in units of nm^2 and "time" is in millions of MC steps. The red line indicates unit slope (diffusive behavior).

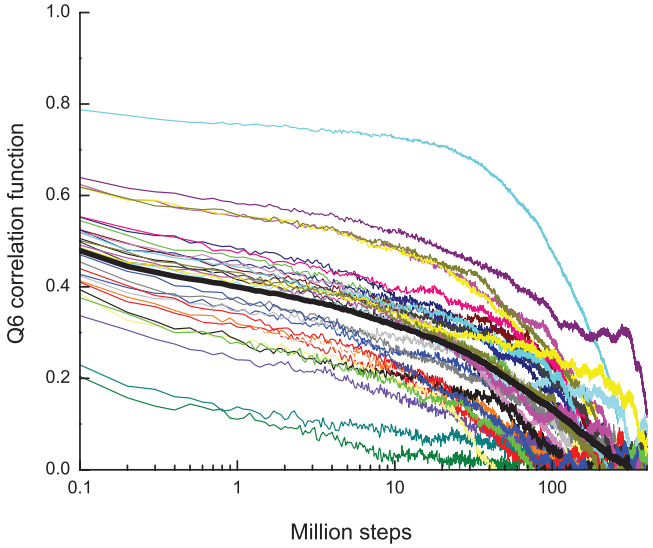

FIG. 9. Q_6 correlation function for 32 parallel independent runs at 228.6 K, 2.2 kbar in the simulation window of $\rho^* = 0.90$ g/cc, $Q_6^* = 0.05$. Each color represents a single run. Black thick line is the average over the 32 runs.

Uncertainties are generally larger in the LDL basin, due to the long relaxation times, but are always within $\pm 0.46\ k_B T$.

B. Time-dependent behavior

Because of the extremely long relaxation times in the LDL phase, we investigated diffusive behavior and structural relaxation to ensure that our free energy calculations were properly equilibrated. Figure 8 shows the mean-squared displacement (in units of nm^2) versus "time" (in millions of single-molecule MC steps), averaged over 32 independent runs at 228.6 K and 2.2 kbar, in the ($\rho^* = 0.9$ g/cc, $Q_6^* = 0.05$ window). Diffusive behavior is attained within approximately 50×10^6 MC steps, and it takes approximately 600×10^6 MC steps for molecules to diffuse a distance of 1 nm (ca. 3 molecular diameters). In each simulation, time origins were spaced 0.3×10^6 MC steps apart.

Figure 9 shows the evolution of the Q_6 time correlation function, defined as

$$C_{Q6}(t) = \frac{\langle Q_6(t)\, Q_6(0)\rangle - \langle Q_6\rangle^2}{\langle Q_6^2\rangle - \langle Q_6\rangle^2}, \tag{8}$$

where $Q_6(t)$ is the Q_6 bond-orientational order parameter at time t and $\langle Q_6\rangle$ is the ensemble average. The calculation was performed at 228.6 K and 2.2 kbar, in the ($\rho^* = 0.9$ g/cc, $Q_6^* = 0.05$ window). In each simulation, time origins were spaced 0.01×10^6 MC steps apart. Shown in the figure are both the evolution of the Q_6 correlation in each of 32 independent simulations and their average (thick black curve). It can be seen that the system exhibits pronounced dynamic heterogeneity, with the relaxation time τ, $C(\tau) = e^{-1}$, ranging from ~2 (average) $\times 10^6$ to ~100 (maximum) $\times 10^6$ MC steps.

The temporal evolution of the self-intermediate scattering function, defined as $F_s(k, t) = \langle \exp[i\boldsymbol{k}\cdot \Delta\boldsymbol{r}(t)]\rangle$, is shown in Figure 10, where $\boldsymbol{k}$ is the wave vector and $\Delta\boldsymbol{r}(t)$ is the displacement experienced by a molecule in a time interval t. This quantity was computed at 228.6 K and 2.2 kbar, in the sampling window $\rho^* = 0.9$ g/cc, $Q_6^* = 0.05$ for two wave vectors, $k\sigma = 5.28$ and 9.29, corresponding to the first two peaks in the static structure factor. The curves shown in Figure 10 are averages over 32 independent runs, in each of which time origins were chosen every 0.3×10^6 steps. Relaxation is slowest at wave vector $k\sigma = 5.28$ and the corresponding relaxation time τ, $F_s(k\sigma = 5.28, \tau) = e^{-1}$ is approximately 20×10^6 MC steps. It follows from Figures 8–10 that structural relaxation in the LDL phase at the lowest temperature investigated in this work is approximately 100×10^6 single-molecule MC steps. This established the criterion for choosing the appropriate length of MC runs in this study. In recent molecular

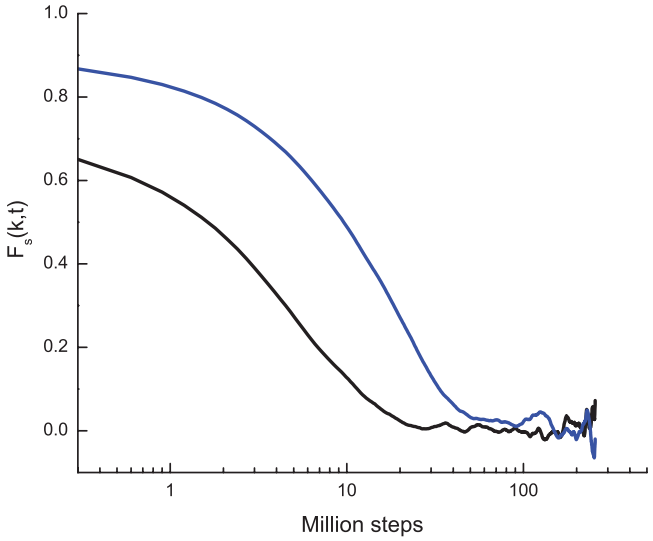

FIG. 10. Self-intermediate scattering function at 228.6 K, 2.2 kbar in the simulation window of $\rho^* = 0.90$ g/cc, $Q_6^* = 0.05$ for wave vectors $k = 5.28\ \sigma^{-1}$ (blue) and $9.29\ \sigma^{-1}$ (black).

Downloaded 06 Dec 2012 to 128.112.34.78. Redistribution subject to AIP license or copyright; see http://jcp.aip.org/about/rights_and_permissions

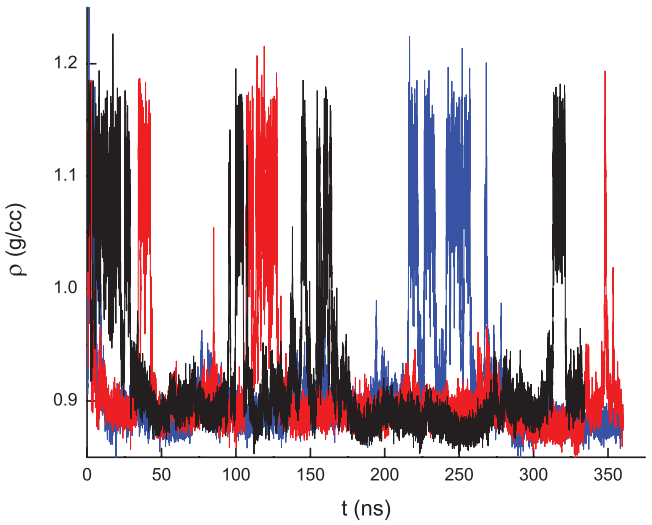

FIG. 11. Time trajectories of three *NPT* molecular dynamics simulations at 235 K and 2 kbar. Note the spontaneous flipping between the LDL and HDL phases.

dynamics studies,[68] relaxation times of the order of 100 ns have been reported for the LDL phase.

Figure 11 shows the system's time-dependent behavior during *NPT* molecular dynamics simulations at 235 K and 2 kbar, a condition close to coexistence according to our free energy calculations (see Figure 4). In very satisfactory agreement with the latter, the system fluctuates between the LDL and HDL phases. Similar behavior has been reported recently by Kesselring *et al.*[68] in the ST2 model with reaction field treatment of long-ranged electrostatic interactions.

C. Effect of Ewald boundary conditions

As stated in Sec. II, we employed vacuum boundary conditions for the Ewald sums in all of our calculations. We have found that using conducting boundary conditions leads to rapid crystallization to a high-density ice phase (ρ ca. 1.5 to 1.7 g/cc) for $T \leq 235$ K and over a broad range of pressures relevant to the present calculations. A typical trajectory is illustrated in Figure 12. The position of the oxygen atoms in the ice phase is consistent with ice VII but, unlike ice VII, the crystal obtained in the simulations invariably contains high dipolar order (Figure 12 inset). This behavior was seen using both our MC and MD in-house codes and has also been observed by other research groups.[77] A similar structure, but without dipolar order, was seen by Creelman and Poole[78] using reaction field treatment of long-ranged electrostatic interactions.[79] Limmer and Chandler employed conducting boundary conditions in their study of the free energy surface of the ST2 model;[64] using hybrid Monte Carlo moves in their simulations, they did not observe the high-density crystal phase. The origin of this discrepancy between our results (Figure 12) and those of Limmer and Chandler (no high-density ice phase) is not well understood at present. We have not been able to reproduce their results.

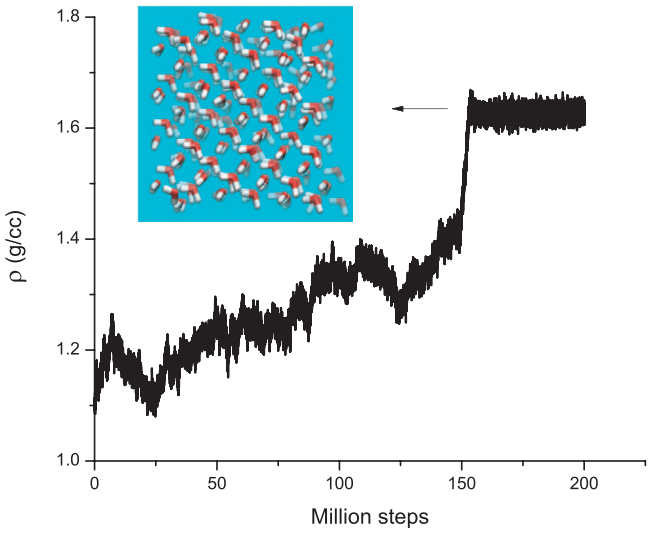

FIG. 12. Effect of Ewald boundary conditions at low temperatures. Time-dependence of the density, illustrating the formation of a high-density, ice VII-like crystal in a typical *NPT*-MC simulation at (228.6 K, 2.2 kbar) using conducting boundary conditions. The inset shows a typical snapshot of the configuration at the end of the simulation. Note the strong dipolar order.

IV. CONCLUSIONS

In this work we have studied the free energy surface of the ST2 model of water[23] with Ewald treatment of long-ranged electrostatics, as a function of density and a bond-orientational order parameter that can distinguish crystalline from amorphous configurations.[65] Calculations were performed at two state points (228.6 K, 2.2 kbar) and (235 K, 2.2 kbar) and reweighed to other thermodynamic conditions. In agreement with our previous results for the same model[59] in which we studied the free energy as a function only of density, we find a phase transition between a low-density and a high-density liquid ($\rho \sim 0.91$ g/cc and $\sim$1.15 g/cc, respectively). The fact that the two basins are contained within the range of bond-orientational order probed in our study ($Q_6 \leq 0.1$) shows that the two phases are amorphous, not crystalline. Structural relaxation and diffusion calculations, furthermore, confirm that both phases are ergodic, not glassy. Although our free energy calculations do not require the structural differentiation of the LDL and HDL phases,[80] both of which lack long-range order, such an analysis would call for the use of additional order parameters.[68]

By limiting our sampling to Q_6 values lower than 0.1, we have imposed a constraint on the free energy surface that we calculate. Metastability is inseparable from constraints: in their absence, the system will evolve irreversibly towards a stable equilibrium state, in this case the crystal. In experiments, a property q of a metastable liquid can be studied provided that the characteristic time τ_q needed to measure the property is appreciably shorter than the time τ_{out} for transformation into the stable phase. Similarly, in simulations, a metastable system can be studied as long as the structural relaxation time needed for adequate sampling of phase space τ_α is appreciably shorter than τ_{out}. In the recent interesting work of Moore and Molinero on a coarse-grained model of water,[70] eventually the supercooled liquid can no longer be equilibrated before it crystallizes (i.e., $\tau_\alpha \sim \tau_{out}$) and there is no sign of a liquid-liquid transition at a more modest

Downloaded 06 Dec 2012 to 128.112.34.78. Redistribution subject to AIP license or copyright; see http://jcp.aip.org/about/rights_and_permissions

supercooling before this condition is reached. In contrast, over the range of conditions studied in our work, the ST2 model exhibits very different behavior, namely, $\tau_{out} \gg \tau_\alpha$ and a liquid-liquid transition is observed. Under these conditions, limiting the range of bond orientational order sampled during the free energy calculation is both physically realistic and computationally expedient, because even during long independent simulations (e.g., O $(30\tau_\alpha)$) the system shows no sign of crystallizing even as its properties fluctuate about their (meta)stable equilibrium values. One therefore expects that computing the full free energy surface, including the high-Q_6 region, will not alter the low-Q_6 region that has been the focus of this work. This calculation is in progress and will be reported separately.

Another important and computationally demanding test is to verify whether the free energy barrier between the two liquid phases (see, e.g., Figure 4) scales as $N^{2/3}$, corresponding to the formation of an interface between the coexisting phases. This calculation requires computing the free energy surface across a range of system sizes. It, too, is in progress and will be reported separately.

The separation of structural relaxation and crystallization times, a prerequisite for performing the type of calculations reported here, is clearly dependent on details of intermolecular interactions that govern the relative rates of phase space sampling and crystal nucleation. Accordingly, the question of the existence of a liquid-liquid transition, or a lack thereof, can only be answered on a case-by-case basis. A recent 3 μs-long simulation of an atomistic model of water under deeply supercooled conditions exhibits a clear separation of relaxation and crystallization time scales such as we report here;[81] the same behavior was observed by Kesselring *et al.*[68] It would be interesting to perform calculations such as the ones reported herein for a range of models representing water and other tetrahedral liquids. This would provide currently lacking information on those aspects of intermolecular interactions that can give rise to a liquid-liquid transition.

The fact that behavior such as is reported in Figure 12 depends sensitively on the choice of Ewald boundary conditions suggests that details of implementation in the treatment of long-ranged electrostatics can have a profound effect on the low-temperature behavior of dipolar systems. The precise reasons underlying this behavior are not well understood and deserve further study.

We close by reiterating that model calculations such as the present one do not address the question of the presence or absence of a liquid-liquid transition in any given specific substance, such as water. At present we do not have classical force fields of sufficient accuracy to address this question, the answer to which must necessarily come from experiments.

ACKNOWLEDGMENTS

P.G.D. gratefully acknowledges the support of the National Science Foundation (Grant No. CHE-1213343) and BP (Carbon Mitigation Initiative at Princeton University). A.Z.P. acknowledges support from the Department of Energy, Office of Basic Energy Sciences, under Grant No. DE-SC0002128. Calculations were performed at the Terascale Infrastructure for Groundbreaking Research in Engineering and Science (TIGRESS) at Princeton University. We gratefully acknowledge C.A. Angell, M.A. Anisimov, P.H. Poole, F. Sciortino, H.E. Stanley, and V. Molinero and, without this implying their agreement with our conclusions, D. Chandler and D. Limmer for helpful discussions; D. Chandler, D. Limmer, P.H. Poole, F. Sciortino, and H.E. Stanley for generously sharing their data with us; and T. Head-Gordon for generously sharing her parallelized MD code with us.

[1] F. Franks, *Water: A Matrix for Life*, 2nd ed. (Royal Society of Chemistry, Cambridge, 2000).
[2] P. Ball, *Life's Matrix. A Biography of Water* (Farrar, Strauss and Giroux, New York, 1999).
[3] C. A. Angell, Annu. Rev. Phys. Chem. **34**, 593 (1983).
[4] P. G. Debenedetti, *Metastable Liquids. Concepts and Principles* (Princeton University Press, Princeton, 1996).
[5] P. G. Debenedetti, J. Phys.: Condens. Matter **15**, R1669 (2003).
[6] P. G. Debenedetti and H. E. Stanley, Phys. Today **56**(6), 40 (2003).
[7] R. J. Speedy and C. A. Angell, J. Chem. Phys. **65**, 851 (1976).
[8] O. Mishima, J. Chem. Phys. **133**, 144503 (2010).
[9] H. Kanno and C. A. Angell, J. Chem. Phys. **70**, 4008 (1979).
[10] C. A. Angell, J. Shuppert, and J. C. Tucker, J. Phys. Chem. **77**, 3092 (1973).
[11] D. H. Rasmussen, A. P. MacKenzie, C. A. Angell, and J. C. Tucker, Science **181**, 342 (1973).
[12] C. A. Angell, M. Oguni, and W. J. Sichina, J. Phys. Chem. **86**, 998 (1982).
[13] D. G. Archer and R. W. Carter, J. Phys. Chem. B **104**, 8563 (2000).
[14] E. Tombari, C. Ferrari, and G. Salvetti, Chem. Phys. Lett. **300**, 749 (1999).
[15] L. Ter Minassian, P. Pruzan, and A. Soulard, J. Chem. Phys. **75**, 3064 (1981).
[16] D. E. Hare and C. M. Sorensen, J. Chem. Phys. **84**, 5085 (1986).
[17] D. E. Hare and C. M. Sorensen, J. Chem. Phys. **87**, 4840 (1987).
[18] T. Koop, B. Luo, A. Tsias, and T. Peter, Nature (London) **406**, 611 (2000).
[19] H. R. Pruppacher, J. Atmos. Sci. **52**, 1924 (1995).
[20] M. B. Baker, Science **276**, 1072 (1997).
[21] F. Madonna, F. Russo, R. Ware, and G. Pappalardo, Geophys. Res. Lett. **36**, L18802, doi:10.1029/2009GL039545 (2009).
[22] P. H. Poole, F. Sciortino, U. Essmann, and H. E. Stanley, Nature (London) **360**, 324 (1992).
[23] F. H. Stillinger and A. Rahman, J. Chem. Phys. **60**, 1545 (1974).
[24] O. Mishima, L. D. Calvert, and E. Whalley, Nature (London) **314**, 76 (1985).
[25] O. Mishima, J. Chem. Phys. **100**, 5910 (1994).
[26] T. Loerting and N. Giovambattista, J. Phys.: Condens. Matter **18**, R919 (2006).
[27] S. Sastry, P. G. Debenedetti, F. Sciortino, and H. E. Stanley, Phys. Rev. E **53**, 6144 (1996).
[28] R. J. Speedy, J. Phys. Chem. **86**, 982 (1982).
[29] K. Stokely, M. G. Mazza, H. E. Stanley, and G. Franzese, Proc. Natl. Acad. Sci. U.S.A. **107**, 1301 (2010).
[30] P. H. Poole, T. Grande, C. A. Angell, and P. F. McMillan, Science **275**, 322 (1997).
[31] O. Mishima and H. E. Stanley, Nature (London) **392**, 164 (1998).
[32] O. Mishima, Phys. Rev. Lett. **85**, 334 (2000).
[33] M. Durandurdu and D. A. Drabold, Phys. Rev. B **66**, 041201 (2002).
[34] Y. Katayama, Y. Inamura, T. Mizutani, M. Yamakata, W. Utsumi, and O. Shimomura, Science **306**, 848 (2004).
[35] A. Ha, I. Cohen, X. Zhao, M. Lee, and D. Kivelson, J. Phys. Chem. **100**, 1 (1996).
[36] A. Hédoux, Y. Guinet, and M. Descamps, Phys. Rev. B **58**, 31 (1998).
[37] R. Kurita and H. Tanaka, Science **306**, 845 (2004).
[38] H. Tanaka, R. Kurita, and H. Mataki, Phys. Rev. Lett. **92**, 025701 (2004).
[39] M. Beye, F. Sorgenfrei, W. F. Schlotter, W. Wurth, and A. Föhlisch, Proc. Natl. Acad. Sci. U.S.A. **107**, 16772 (2010).
[40] D. Liu, Y. Zhang, C.-C. Chen, C.-Y. Mou, P. H. Poole, and S.-H. Chen, Proc. Natl. Acad. Sci. U.S.A. **104**, 9570 (2007).
[41] F. Mallamace, C. Corsaro, M. Broccio, C. Branca, N. González-Segredo, J. Spooren, S.-H. Chen, and H. E. Stanley, Proc. Natl. Acad. Sci. U.S.A. **105**, 12725 (2008).
[42] Y. Zhang, A. Faraone, W. A. Kamitakahara, K.-H. Liu, C.-Y. Mou, J. B. Leao, S. Chang, and S.-H. Chen, Proc. Natl. Acad. Sci. U.S.A. **108**, 12206 (2011).

Downloaded 06 Dec 2012 to 128.112.34.78. Redistribution subject to AIP license or copyright; see http://jcp.aip.org/about/rights_and_permissions

[43]J. Swenson, Phys. Rev. Lett. **97**, 189801 (2006).
[44]P. H. Poole, F. Sciortino, T. Grande, H. E. Stanley, and C. A. Angell, Phys. Rev. Lett. **73**, 1632 (1994).
[45]T. M. Truskett, P. G. Debenedetti, S. Sastry, and S. Torquato, J. Chem. Phys. **111**, 2647 (1999).
[46]G. Franzese, M. I. Marqués, and H. E. Stanley, Phys. Rev. E **67**, 011103 (2003).
[47]T. M. Truskett and K. A. Dill, J. Chem. Phys. **117**, 5101 (2002).
[48]D. A. Fuentevilla and M. A. Anisimov, Phys. Rev. Lett. **97**, 195702 (2006).
[49]C. E. Bertrand and M. A. Anisimov, J. Phys. Chem. B **115**, 14099 (2011).
[50]V. Holten, C. E. Bertrand, M. A. Anisimov, and J. V. Sengers, J. Chem. Phys. **136**, 094507 (2012).
[51]V. Holten and M. A. Anisimov, Sci. Rep. **2**, 713 (2012).
[52]S. Harrington, S. Zhang, P. H. Poole, F. Sciortino, and H. E. Stanley, Phys. Rev. Lett. **78**, 2409 (1997).
[53]M. Yamada, H. E. Stanley, and F. Sciortino, Phys. Rev. E **67**, 010202 (2003).
[54]M. Yamada, S. Mossa, H. E. Stanley, and F. Sciortino, Phys. Rev. Lett. **88**, 195701 (2002).
[55]P. H. Poole, I. Saika-Voivod, and F. Sciortino, J. Phys.: Condens. Matter **17**, L431 (2005).
[56]D. Paschek, Phys. Rev. Lett. **94**, 217802 (2005).
[57]P. Jedlovszky and R. Vallauri, J. Chem. Phys. **122**, 081101 (2005).
[58]J. L. F. Abascal and C. Vega, J. Chem. Phys. **133**, 234502 (2010).
[59]Y. Liu, A. Z. Panagiotopoulos, and P. G. Debenedetti, J. Chem. Phys. **131**, 104508 (2009).
[60]A. Z. Panagiotopoulos, J. Phys.: Condens. Matter **12**, R25 (2000).
[61]D. Frenkel and B. Smit, *Understanding Molecular Simulation: From Algorithms to Applications*, 2nd ed. (Academic, New York, 2002).
[62]F. Sciortino, I. Saika-Voivod, and P. H. Poole, Phys. Chem. Chem. Phys. **13**, 19759 (2011).
[63]H. J. C. Berendsen, J. R. Griguera, and T. P. Straatsma, J. Phys. Chem. **91**, 6269 (1987).
[64]D. Limmer and D. Chandler, J. Chem. Phys. **135**, 134503 (2011).
[65]P. J. Steinhardt, D. R. Nelson, and M. Ronchetti, Phys. Rev. B **28**, 784 (1983).
[66]M. R. Shirts and J. D. Chodera, J. Chem. Phys. **129**, 124105 (2008).
[67]V. Molinero and E. B. Moore, J. Phys. Chem. B **113**, 4008 (2009).
[68]T. A. Kesselring, G. Franzese, S. V. Buldyrev, H. J. Herrmann, and H. E. Stanley, Sci. Rep. **2**, 474 (2012).
[69]E. B. Moore and V. Molinero, J. Chem. Phys. **130**, 244505 (2009).
[70]E. B. Moore and V. Molinero, Nature (London) **479**, 506 (2011).
[71]S. B. Kiselev, Int. J. Thermophys. **22**, 1421 (2001).
[72]S. B. Kiselev and J. F. Ely, J. Chem. Phys. **116**, 5657 (2002).
[73]S. Kumar, D. Bouzida, R. H. Swendsen, P. A. Kollman, and J. M. Rosenberg, J. Comput. Chem. **13**, 1011 (1992).
[74]H W. Horn, W. C. Swope, J. W. Pitera, J. D. Madura, T. J. Dick, G. L. Hura, and T. Head-Gordon, J. Chem. Phys. **120**, 9665 (2004).
[75]G. J. Martyna, Mol. Phys. **87**, 1117 (1996).
[76]H. C. Andersen, J. Comput. Phys. **52**, 24 (1983).
[77]E. Lascaris, C. Zhang, G. Franzese, G. Galli, and H. E. Stanley, private communication (2012).
[78]C. Creelman and P. H. Poole, private communication (2012).
[79]M. P. Allen and D. J. Tildesley, *Computer Simulations of Liquids* (Oxford University Press, Oxford, 1987).
[80]A. K. Soper and M. A. Ricci, Phys. Rev. Lett. **84**, 2881 (2000).
[81]R. Shevchuk and F. Rao, J. Chem. Phys. **137**, 036101 (2012).

Downloaded 06 Dec 2012 to 128.112.34.78. Redistribution subject to AIP license or copyright; see http://jcp.aip.org/about/rights_and_permissions